Use of fast-Fourier-transform computational methods in radiation transport

Burke Ritchie, Pieter G. Dykema, and Dennis Braddy
Lawrence Livermore National Laboratory, University of California, Livermore, California 94550
(Received 15 April 1996; revised manuscript received 18 October 1996)

Fast-Fourier-transform computational methods are used to solve the radiation-transport equation. Results are presented in nondiffusive and diffusive regimes. In the latter regime the method is benchmarked against the Schrödinger equation, which has the form of a diffusion equation in imaginary time. The method is further tested against prototypical problems in radiation transport. [S1063-651X(97)02808-0]

PACS number(s): 02.70.−c, 51.50.+v

I. INTRODUCTION

Fast-Fourier-transform (FFT) methods have been used extensively in optical [1] and quantum [2] physics and are remarkable for their computational speed and numerical stability. Also, FFT routines are readily available in one to three dimensions (although only for Cartesian coordinates) and can be used quite flexibly in a variety of numerical procedures. In this paper we show that FFT methods are also useful in solving the radiation-transport equation

$$\left(\frac{1}{c}\frac{\partial}{\partial t}+\vec{\Omega}\cdot\vec{\nabla}+\kappa\right)I(\vec{r},\vec{\Omega})=\kappa_a B+\frac{\kappa_s}{4\pi}\int d\vec{\Omega}' I(\vec{r},\vec{\Omega}'), \tag{1a}$$

$$\kappa=\kappa_a+\kappa_s, \tag{1b}$$

where I is the radiation intensity per unit frequency in ergs cm^{-2}, κ_a and κ_s are the absorptive and scattering opacities, respectively, $\vec{\Omega}$ is the unit vector in the light-ray direction, and B is the Planckian source

$$B=2\frac{h\nu^3}{c^2}(e^{h\nu/kT}-1)^{-1}. \tag{2}$$

Equation (1a) is also parametrically a function of the light frequency ν. The form of the second term on the right-hand side of Eq. (1a) is appropriate for isotropic scattering. FFT methods already have been used to solve the Navier-Stokes equation [3], but not, to our knowledge, the transport equation; the latter, however, has been studied recently using finite-element methods [4].

II. GENERAL CONSIDERATIONS

In virtually all FFT methods the spatial derivatives of an equation are Fourier transformed analytically and the temporal advance is carried out in transform space. This procedure has the effect that spatial derivatives, which in real-space, finite-difference methods are distributed locally over a selected number of grid zones and can be the source of numerical instabilities, are smoothed globally over all space, thereby leading to robustly stable results. Also there is a practical computational advantage in that the Crank-Nicolson method [5,6] can be used to split the operator between the advanced and retarded parts of the temporally differenced solution and then, in transform space, the left-hand side can be inverted in a single scalar operation even in three dimensions.

In the implementation of FFT methods to Eq. (1a) products of two functions of space, such as the opacity and intensity in Eq. (1a), are treated explicitly, that is, by assuming that such products are known from a prior time step so that they are Fourier transformed as products, thereby averting convolution integrals and an intractable six-dimensional (6D) numerical problem. However, this scheme is not practical for optically thick problems, for which an implicit scheme is proposed and implemented.

The use of FFT methods in quantum physics [2] suggests that these methods would be useful in the diffusive limit of radiation transport because the Schrödinger equation has the form of a diffusion equation in imaginary time and its integration in imaginary time actually has been used as a practical computational method [7] to calculate, for an electron bound in an attractive potential, the diffusion of an assumed initial wave form into the quantum eigenfunction, with accompanying determination of the eigenenergy. This suggests that one may use the Schrödinger equation itself to benchmark numerical procedures used in the diffusive limit of the radiation-transport equation. One may then reasonably expect that such procedures would also be valid in the nondiffusive regime. Conversely, in a.u., for which $\hbar=e=m=1$, the scaled Schrödinger equation behaves like an imaginary-time diffusion equation on macroscopic scales actually encountered in practical applications. The nature of the imaginary-time solutions for the diffusion equation (i.e., the real-time Schrödinger equation) is primarily oscillatory, rather than monotonic, in the regime of interest; thus we find that the Schrödinger test tends to be more stringent in terms of temporal-spatial zone refinement than that of real-time diffusion-equation solutions.

The advantage of choosing the Schrödinger benchmark is its known spectra of eigenstates for a variety of potentials, calculated using quite independent computational methods, and the sensitivity of the spectrum and conservation of the wave-function norm to the accuracy of one's numerical methods. Also the Schrödinger benchmark is available in three dimensions. One may, with some justification, object that the Schrödinger benchmark suffers by not belonging to the actual transport problem one is solving; however, the benchmarks that are available in the appropriate regime, for example, analytically solvable 1D problems, do not test the full range of numerical procedures that are used in 2D and

3D applications. We do not limit this study to the Schrödinger benchmark, however, but also present results for standard radiation-transport applications.

Finally, in Fourier transforming Eq. (1) we assume that the intensity vanishes at the grid boundaries, thereby eliminating the presence of surface terms in the Fourier transforms of the spatial derivatives. In problems in which this assumption cannot be made because, for example, of opacity variations between different material boundaries that are large on the scale of grid resolution within a given material, one could make use of the methods proposed and tested for layered dielectric media [8], where it is found that in an algorithm to advance the solution temporally over an interval dt surface terms contribute to order dt^2 and hence can be dropped in a first-order accurate scheme. The way to avoid such terms [1,2,7] is to contain the system one is simulating in a box with absorptive walls. The absorption of flux by the walls eliminates numerical reflection of flux back into the interior of the box from the grid boundaries. If the size of the problem is such that this is impractical, then the suitability of FFT methods for such problems would have to be reevaluated on a case by case basis.

III. COMPUTATIONAL ALGORITHMS

In optically thin regimes our algorithm involves solving the transform equation

$$\left(\frac{1}{c}\frac{\partial}{\partial t}-i\vec{\Omega}\cdot\vec{k}\right)\tilde{I}(\vec{k},\Omega)=\tilde{R}(\vec{k},\Omega), \tag{3}$$

where the tilde designates the spatial Fourier transform and the right-hand side of Eq. (3) is the Fourier transform of all terms in Eq. (1a) except the first two terms on the left-hand side. Next we difference Eq. (3) temporally and split the k-space operator between the advanced and retarded transform-space solutions; this is just the Crank-Nicolson method in transform space. We obtain

$$\left(1-i\frac{cdt}{2}\vec{\Omega}\cdot\vec{k}\right)\tilde{I}_a=\left(1+i\frac{cdt}{2}\vec{\Omega}\cdot\vec{k}\right)\tilde{I}_r+cdt\tilde{R}(\vec{k},\vec{\Omega}), \tag{4}$$

where the k vector is also discretized on a uniform grid as determined from one's preselection of a uniform spatial grid and use of a standard library FFT routine, which is based on the algorithm of Cooley and Turkey [9]. The method is implemented as follows: forward transformation, advance the transformed solution according to Eq. (4) one step in time, and back transformation. This constitutes one cycle.

In optically thick regimes the explicit treatment of the opacity terms in Eqs. (3) and (4) is unsatisfactory since one is stuck with a Courant-limited scheme in which satisfying the inequality $cdt<\kappa^{-1}$, for example, is not practical in realistic problems; therefore, we propose and test an implicit scheme [10], which has a kinship with the split-operator scheme of [2] and with implicit spatial differencing schemes [6]. We illustrate the method by assuming only absorptive opacities; however, scattering opacity terms can be made implicit in a similar way but require a matrix inversion at each temporal interval to determine the advanced solution.

The temporal interval is divided into the three subintervals, and the advancing algorithm is

$$\left(1-i\frac{cdt}{2}\vec{\Omega}\cdot\vec{k}\right)\tilde{I}_{1/3}=\tilde{I}_0+cdt\tilde{S}(\vec{k}), \tag{5a}$$

$$(1+cdt\kappa_a)I_{2/3}=I_{1/3}, \tag{5b}$$

$$\left(1-i\frac{cdt}{2}\vec{\Omega}\cdot\vec{k}\right)\tilde{I}_1=\tilde{I}_{2/3}, \tag{5c}$$

where S in Eq. (5a) is the source term in Eq. (1a). Equations (5a) and (5c) are written in transform space in order to invert the left-hand sides, and Eq. (5b) is written in real space. If one writes all three equations in real space and operates successively on both sides of Eq. (5c) with the left-hand operators of Eqs. (5a) and (5b), then it is clear that to first order in cdt the following algorithm advances the solution from 0 to 1:

$$(1+cdt\vec{\Omega}\cdot\vec{\nabla}+cdt\kappa_a)I_1=I_0+cdtS. \tag{6}$$

In problems in which the opacity can vary by orders of magnitude as a function of temperature, which can be very nonuniform spatially, one would want a single algorithm for both optically thick and thin regimes. The algorithm given by Eqs. (5) and (6) seems to satisfy this need: it is found to be stable for coarse temporal grids for optically thick applications and it agrees to acceptable accuracy with the optically thin algorithm given by Eqs. (3) and (4).

The algorithm given by Eqs. (5) and (6) is similar to implicit spatial finite-difference schemes, which are desirable to achieve numerical robustness in optically thick media, in the sense that the local opacity and advection terms are brought to the left-hand side of the equation. The difference in the present scheme is the evaluation of the advection terms in transform space by the split-operator scheme given by Eqs. (5). The advantages, as mentioned earlier, are the smoothing effect of globally representing the spatial derivatives in transform space and the scalar rather than matrix form of the operators that must be inverted to calculate the advanced solution.

We also consider that the material medium can be characterized by the temperature distributed over space

$$C_v\frac{\partial T}{\partial t}=\kappa_a\left(\int d\vec{\Omega}\,d\nu\,I-aT^4\right), \tag{7}$$

where C_v is the heat capacity and $a=\pi^2k^4/15\hbar^3c^2$, where k is the Boltzmann constant. This equation is solved using either of two algorithms (where the heat capacity is taken to be constant). In the first the T^4 term is split between the advanced and retarded pieces as $T_aT_r^3$ and then Eq. (7) is solved formally by finding the integrating factor, thereby reducing the numerical problem to temporal integrals. In the second the T^4 term is expanded to first order in a Taylor series about the retarded solution; this procedure linearizes the term in the advanced solution so that part of it can be brought to the left-hand side of the differenced form of Eq. (7). These two algorithms give results that agree mutually

and correctly give the steady solution for a simple test equation in which the first term on the right-hand side of Eq. (7) is a constant.

Equation (1a) is solved for all light-ray directions into the solid angle Ω. The discretization of the equation over Ω, called the discrete ordinates or S_N method, is often used [4,11]. It is based [11] on using geometrically preselected discrete quadrature sets (S_2, S_4,...), which result in $N(N+2)$ light trajectories. This method is based on purely geometrical considerations for the discretization of angle space. Physically, however, we are justified in choosing the initial light-ray directions using a random number generator if the source emits radiation with equal probability in all directions. A number n of initially randomly directed trajectories constitutes an ensemble, and the radiation distribution is represented by the ensemble average, in analogy to classical particle dynamics. The ensemble average is physically equivalent to the S_N approximation to the surface integral, that is,

$$\frac{1}{4\pi}\int d\vec{\Omega}\, I(\vec{r},\vec{\Omega}) \cong \sum w_m I_m(\vec{r},\omega_m) \Rightarrow \frac{1}{n}\sum I_j(\vec{r},\Omega_j), \tag{8}$$

where $\{w_m,\omega_m\}$is the set of quadrature weights and direction cosines [11], respectively, for a given order N of S_N and the last term is the ensemble average over n initially randomly directed trajectories; however, it is not itself a discretization scheme for numerical quadrature. We are motivated by the thought that for the paucity of trajectories due to practical limitations in computer storage the radiation angular distribution may be better simulated by a choice of trajectories whose initial directions match those of the isotropic source than by a choice of trajectories whose directions are fixed by a numerical quadrature scheme and chosen for accuracy of the integrated or total radiation distribution. We test this hypothesis by numerical comparisons. It turns out that for media with strong scattering opacity the S_N appears to be superior to the random method (hereafter call ''hybrid'' for mixed deterministic Monte Carlo) for very low order ($N=4$) because strong scattering induces strong isotropy in the radiation distribution, which is reasonably well represented by low-order S_N quadrature. However, in media with strong absorption and negligible scattering, both methods reflect the paucity of trajectories, but the distortion in the radiation distribution is irregular for the hybrid method and regular or geometric for S_N.

Unfortunately, such distortion or ''ray effect'' is characteristic of transport calculations, reflecting the discretization of the solid angle into which radiation is emitted. We show how the distribution ought to look in the absorptive regime by solving the Maxwell wave equation in the limit of geometric optics, where the wavelength is chosen to be small compared to the smallest structure one wishes to resolve in the transport problem, and application of a spatial filter to eliminate small-scale coherent structures or ''noise.'' It turns out that one can approximately fill all of space in wave theory, which is not decomposed into its Fourier components, with a fraction of the computer storage because all directions are implicitly contained in a single solution.

Returning to our ''hybrid'' transport method, we represent the scalar product in transform space as

$$\vec{\Omega}\cdot\vec{k} = \hat{k}_{xj}k_x + \hat{k}_{yj}k_y + \hat{k}_{zj}k_z, \tag{9}$$

where the careted k's are the set of random numbers chosen in the interval from -1 to 1 with the constraint that the sum of their squares is equal to 1; thus the random choices of two of them fixes the value of the third. The applications below are for 2D problems in a plane, say, in x and z, so that the constraint on the careted k's is that the sum of their squares be less than or equal to one. The uncareted k's are the variables in transform space. Thus a complete calculation is carried out in space and time for each choice j and the intensity distribution is then represented by the ensemble average.

IV. NUMERICAL RESULTS

In a medium dominated by isotropic scattering radiation transport can be described approximately by a single diffusion equation [12]

$$\left(\frac{1}{c}\frac{\partial}{\partial t} - \frac{1}{3\kappa}\nabla^2\right)E = \frac{4\pi}{c}\,\kappa_a B - \kappa_a E, \tag{10a}$$

$$E = \frac{1}{c}\int d\vec{\Omega}\, I(\vec{r},\vec{\Omega}), \tag{10b}$$

where E is the energy density per unit frequency in ergs cm^{-3} s. In Eq. (10a) κ has been written as independent of space to emphasize that the equation has the standard diffusion form; however, in our actual transport calculations κ is a function of space. As discussed earlier, the Schrödinger equation (in a.u.)

$$\left(i\,\frac{\partial}{\partial t} + \frac{1}{2}\nabla^2\right)\psi = V\psi, \tag{11}$$

if expressed on the imaginary time axis [7] $\tau = it$, has the form of Eq. (10a) without the source term, with cdt replaced by $d\tau$ and other obvious replacements. Thus it seems reasonable to benchmark our numerical procedures against solutions of Eq. (11) of known accuracy. In particular we make use of the known spectrum for the time-dependent 1D Schrödinger equation for the so-called soft Coulomb potential model,

$$V = \frac{-1}{\sqrt{1+x^2}}. \tag{12}$$

The Schrödinger equation is solved using the same procedures outlined above for the transport equation and the spectral power (Fig. 1) is calculated using the methods of [2], which principally involve finding the temporal Fourier transform of the overlap integral of ψ at time t with ψ at initial time.

The initial wave function was taken to be the product of a Gaussian and a polynomial even (top) and odd (bottom) with respect to inversion through the origin. For a spatial interval $-25<x<25$, 257 mesh points were used, and for a temporal interval $0<t<10^3$, 10^5 mesh points were used. In Fig. 1 (top) the positions of the spectral peaks of the ground and first excited gerade states and in Fig. 1 (bottom) the position of the first excited ungerade state are in excellent agreement (Table I) with the eigenvalues calculated by the conventional numerical solution of the time-independent Schrödinger

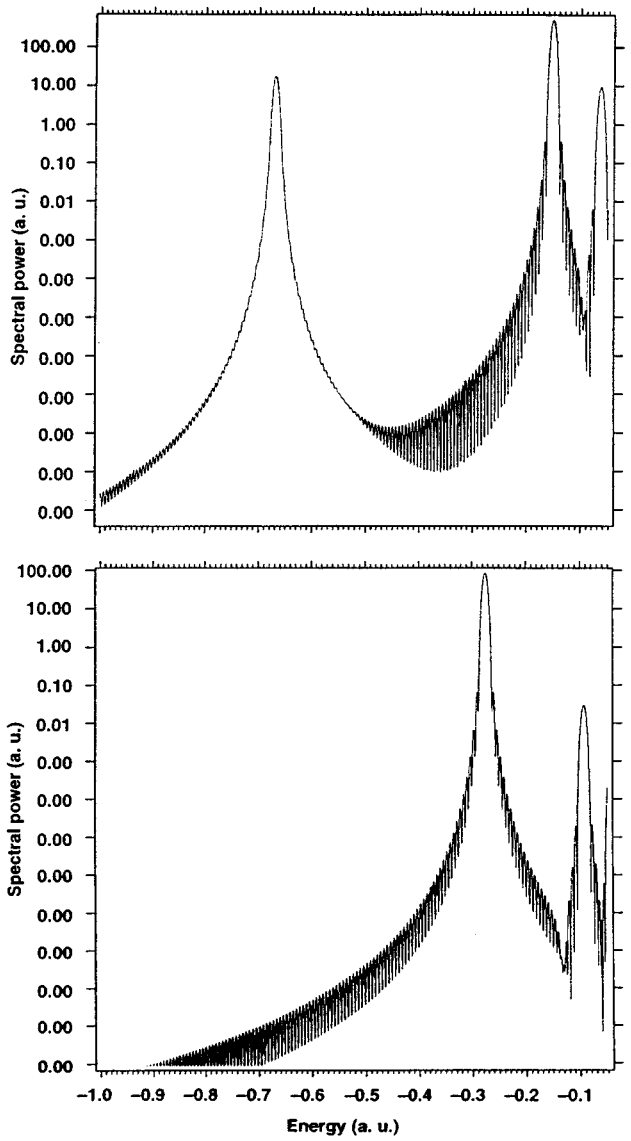

FIG. 1. Time-dependent Schrödinger equation spectral power. Note that the peak positions occur at the eigenvalues in Table I. Top, gerade symmetry; bottom, ungerade symmetry.

equation, where the eigenvalues are determined by integrating forward and backward from the asymptotic region of the potential with trial energies and matching at the origin to obtain zero Wronskians. The ground-state eigenvalue has also been calculated by others [13] and is in excellent agreement with our results. Only the first two gerade and the first ungerade peaks of Fig. 1 are considered accurate because of the adequate size of the spatial interval for these states.

The accuracy of the results of Fig. 1 were achieved at the expense of a considerable temporal grid refinement necessitated by the explicit treatment of the right-hand side of Eq. (8). However, we find that the same accuracy can be achieved using one-tenth the number of temporal zones by using the Heun predictor-corrector method [14], which at each temporal zone uses the first result as a predictor step and then in a corrector step re-solves the differenced equation in which the right-hand side is an average of terms calculated using the retarded and predictor solutions. Since a

TABLE I. Eigenvalues of the time-independent Schrödinger equation (in a.u.) obtained using forward-backward integration with matching for zero Wronskian at the origin.

States	Eigenvalues (this work)	Eigenvalues (Ref. [12])
1	−0.6698	−0.6692
2	−0.2749	
3	−0.1515	

FFT cycle must be used twice for one-tenth the number of temporal zones, this is a fivefold gain in efficiency. However, in the radiation-transport examples that follow we find that acceptable accuracy is achieved for the coarser temporal grid without using the Heun iteration. The reason likely derives from the fact that transport occurs in a monotonic rather than oscillatory regime of the solution.

As a test of our procedures for nondiffusive radiation transport [algorithm given by Eqs. (3) and (4)] we solve the Mordant problem [4,15] (Figs. 2–12), in which an emissive region (with $\kappa_a=10$, $\kappa_s=0$, and unit Planck function) surrounds an absorbing central region ($\kappa_a=5$, $\kappa_s=0$, and zero Planck function). In our version of the problem the region outside the square emitter is free space except for a region of absorption near the grid boundaries. The problem is a good test of numerical methods because the intensity drops very rapidly into the cold absorber in the center, and many methods produce ringing and negative intensities (Gibbs oscillations).

In these calculations 101 temporal points are used for $ct_{\max}=10$ cm, and 128×128 spatial points are used for the two Cartesian directions in centimeters shown in the figures. Figures 2 and 3 compare results respectively for the hybrid method (using 12 trajectories) and the S_N method for $N=4$ [for which in a plane there are $N(N+2)/2$ trajectories]. The S_N method characteristically suffers from a spurious intensity undulation or ray effect in the region of free space surrounding the square emissive region. The hybrid method also shows much irregular distortion for only 12 trajectories. Figures 4 and 5 show the same comparison but with unit scattering opacity ($\kappa_s=1$) in the outside region. Here S_N clearly shows less distortion than the hybrid method. The strong mixing of the light trajectories induced by scattering drives the angular distribution strongly toward isotropy such that the S_N quadrature distribution, which is optimized for integrating the angular distribution over a spherical surface, shows less distortion than the hybrid method for the same small number of trajectories. In Figs. 6–9, however, the hybrid and S_N results, for 40 trajectories each, appear to have comparable distortion without scattering and comparable isotropy with scattering. Figure 10 shows a 500-trajectory hybrid result without scattering, which we would expect to show quite small differences with the corresponding S_N with order $N=\sqrt{1000}$. Thus the advantage of the hybrid method over S_N lies in the ease of its implementation by the use of a random number generator rather than fixed discrete ordinate quadrature sets from tables [11].

How should the angular distribution look for the Mordant problem? The Maxwell wave equation [16]

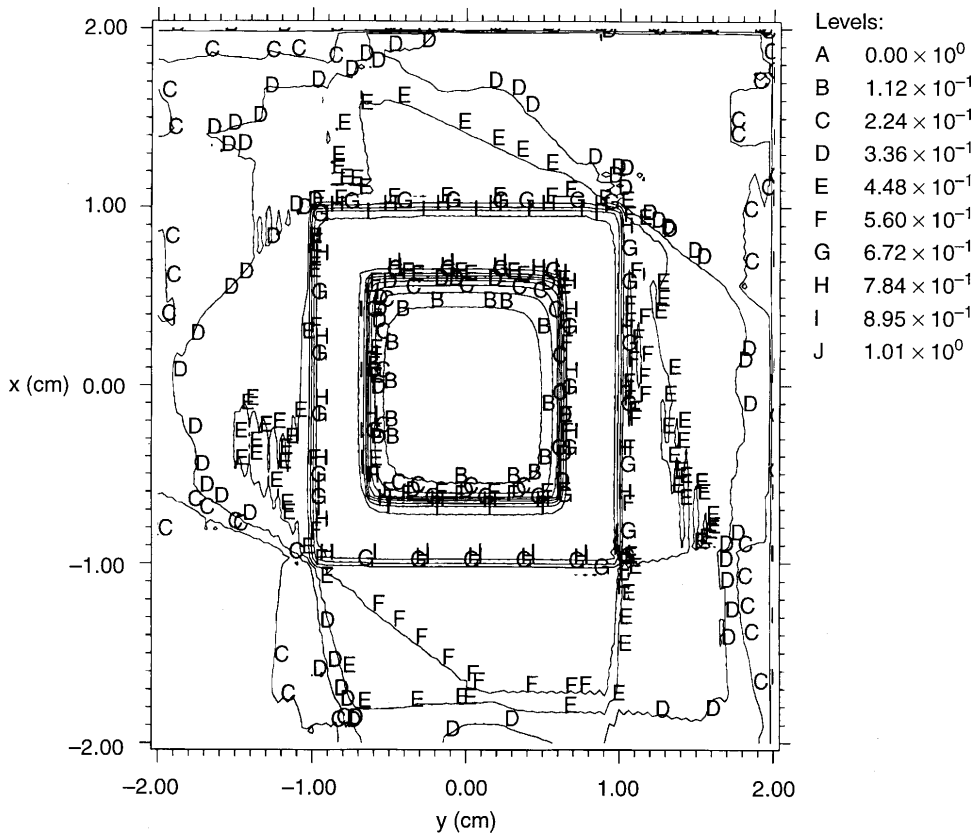

FIG. 2. Radiation distribution using the hybrid method with 12 light trajectories; there is zero scattering opacity.

$$\left(\nabla^2-\frac{1}{c^2}\frac{\partial^2}{\partial t^2}\right)E=\kappa_a\frac{1}{c}\frac{\partial E}{\partial t}, \tag{13}$$

which is undecomposed into its Fourier components, would give us this information if we could resolve the millions of wave oscillations over a centimeter or so of path length. Instead, one can expand the electric field in a single temporal Fourier component

$$E=Ee^{-i\omega t}+E^*e^{i\omega t} \tag{14}$$

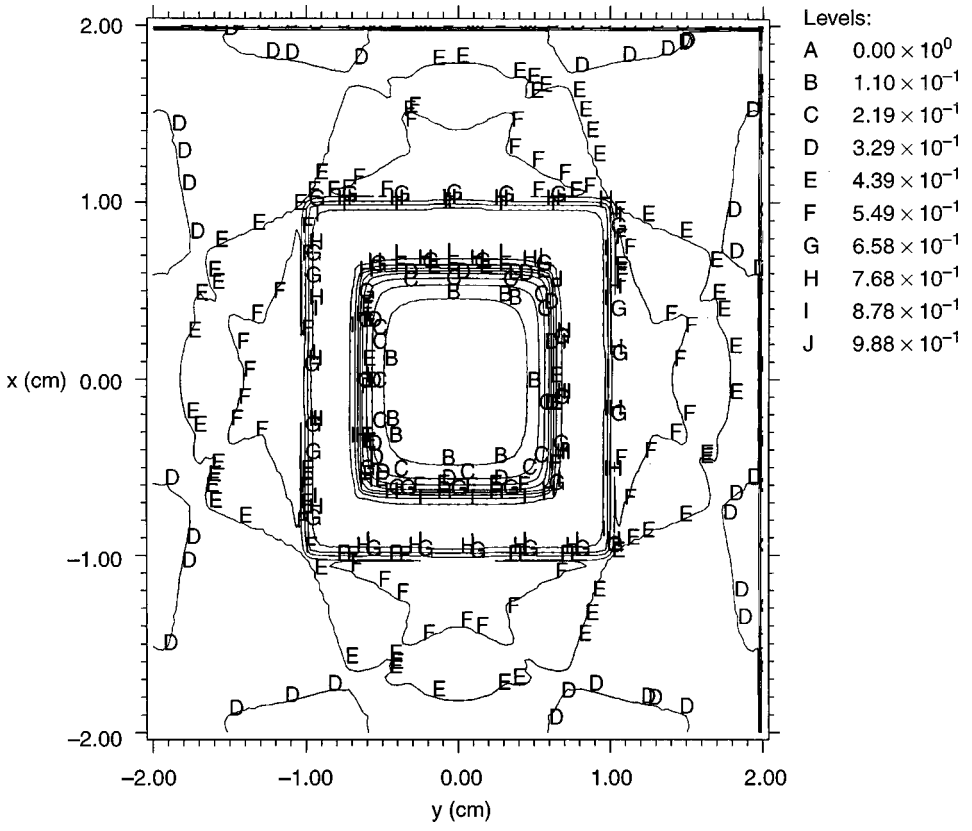

FIG. 3. Radiation distribution using the S_4 method with $4(4+2)/2$ discrete quadrature points; there is zero scattering opacity.

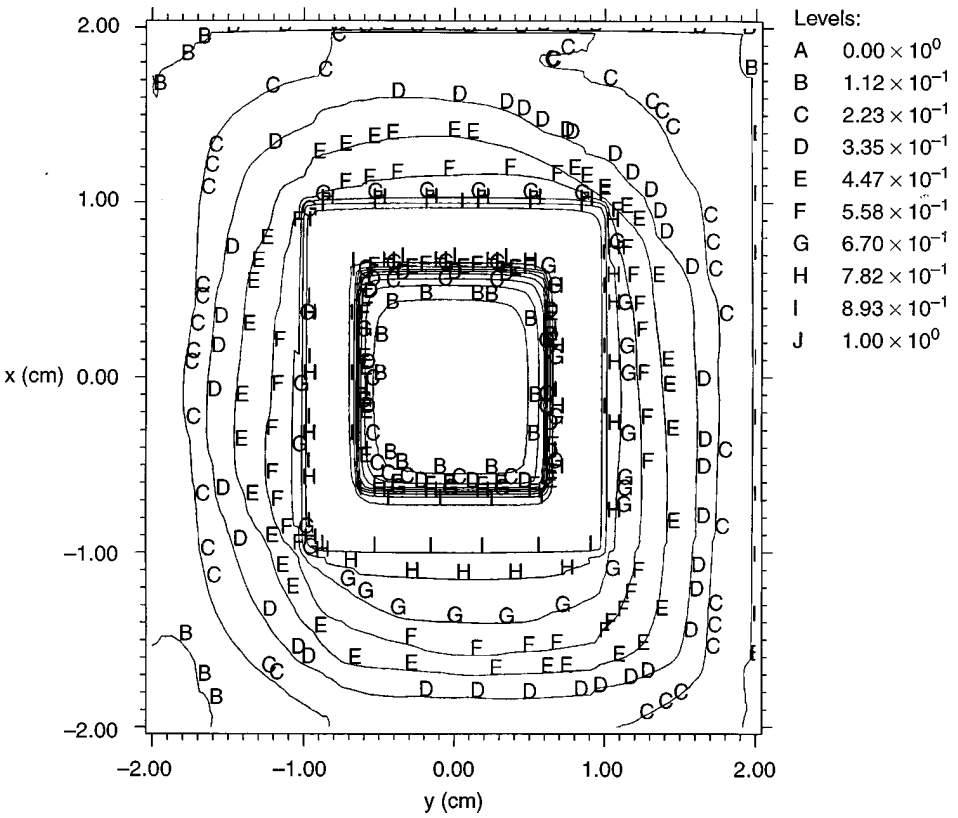

FIG. 4. Radiation distribution using the hybrid method with 12 light trajectories; there is nonzero scattering opacity.

and solve the equation for the envelope

$$\left(\nabla^2+2ik\,\frac{1}{c}\,\frac{\partial}{\partial t}+k^2\right)E=-ik\kappa_a E \tag{15}$$

by choosing a wavelength $\lambda=2\pi/k$ that is small compared to the smallest structure one wishes to resolve in a transport calculation. Equation (15) must be augmented by a source. It may be possible to derive a source from fundamental consid-

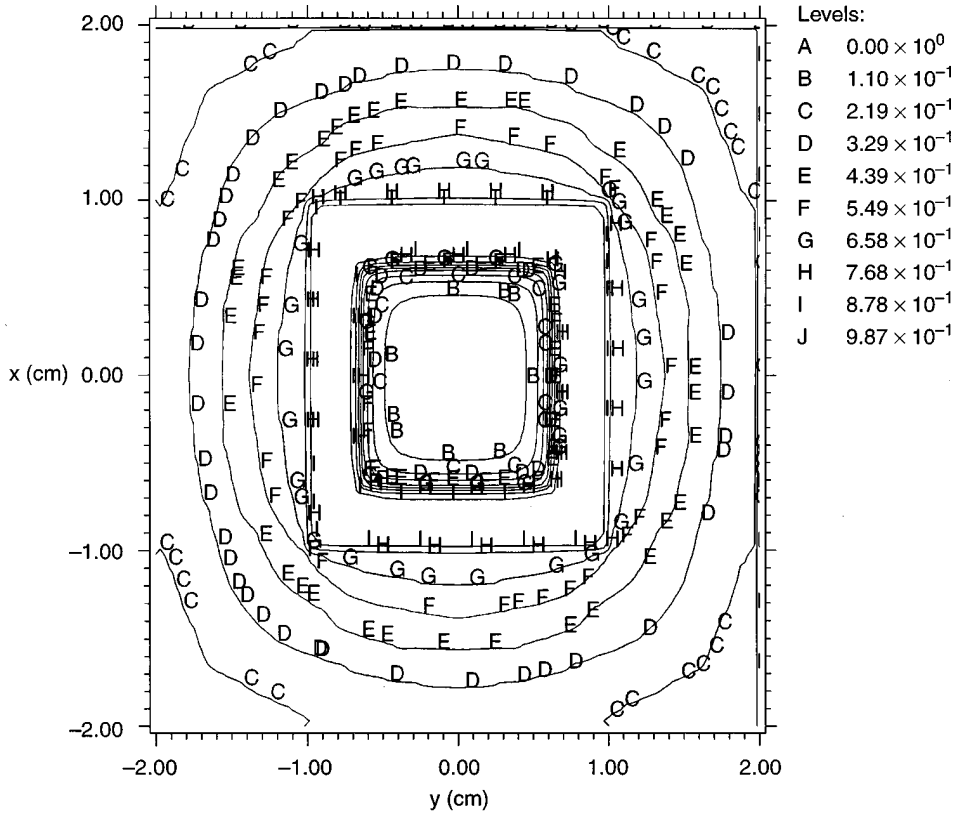

FIG. 5. Radiation distribution using the S_4 method with 4(4+2)/2 discrete quadrature points; there is nonzero scattering opacity.

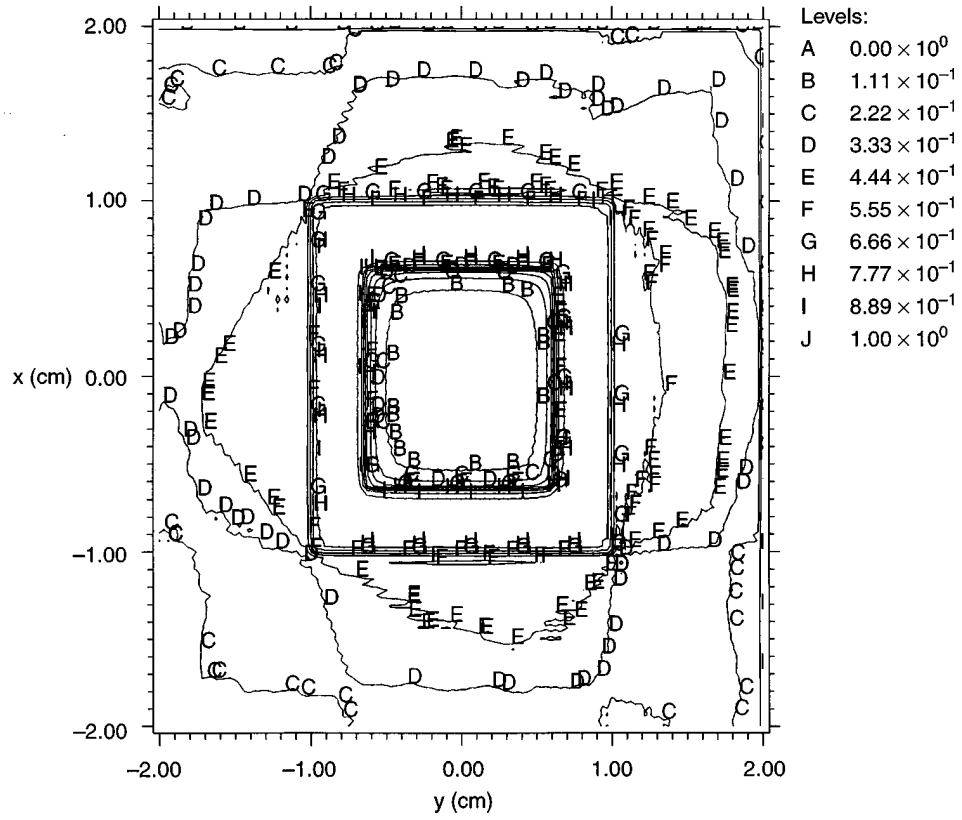

FIG. 6. Radiation distribution using the hybrid method with 40 light trajectories; there is zero scattering opacity.

erations, as in amplified spontaneous emission [17]; here we assume the form $ik\kappa_a A e^{i\vec{k}\cdot\vec{r}}$, where the amplitude A is determined by normalizing the intensity, which is the time average of E^2, at each time step to the source we used in the transport problem. The directions of the wave vector are calculated at every time step using a random number generator and the selection criteria discussed earlier for hybrid transport [Eq. (9)].

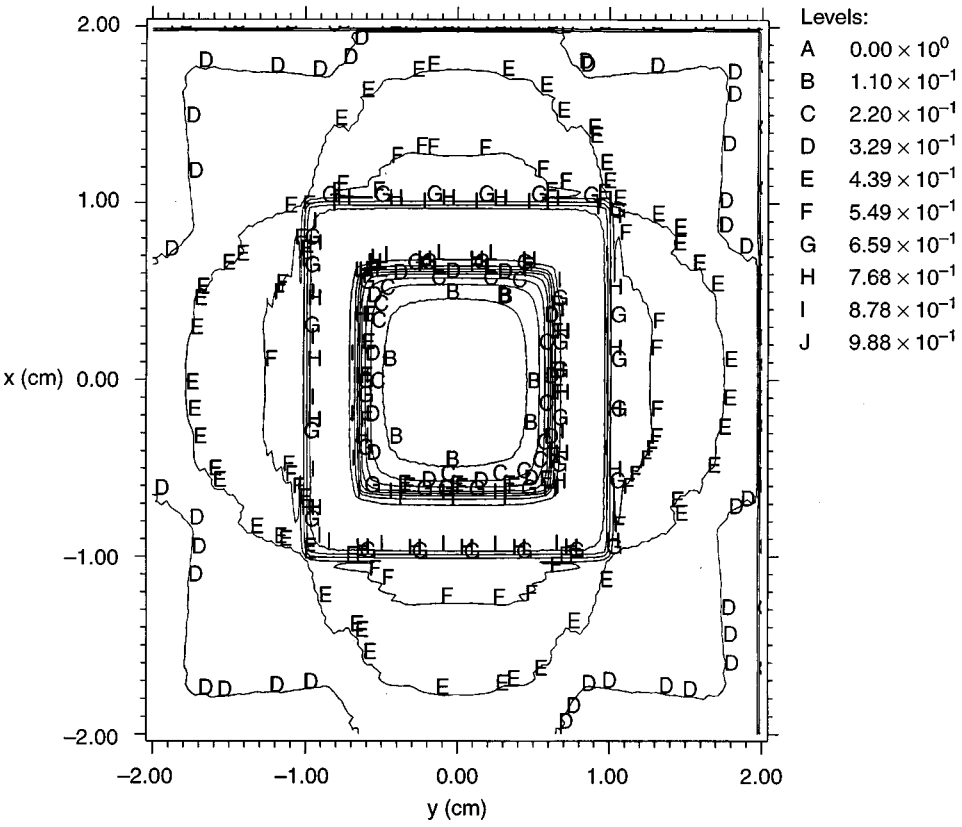

FIG. 7. Radiation distribution using the S_8 method with 8(8 +2)/2 discrete quadrature points; there is zero scattering opacity.

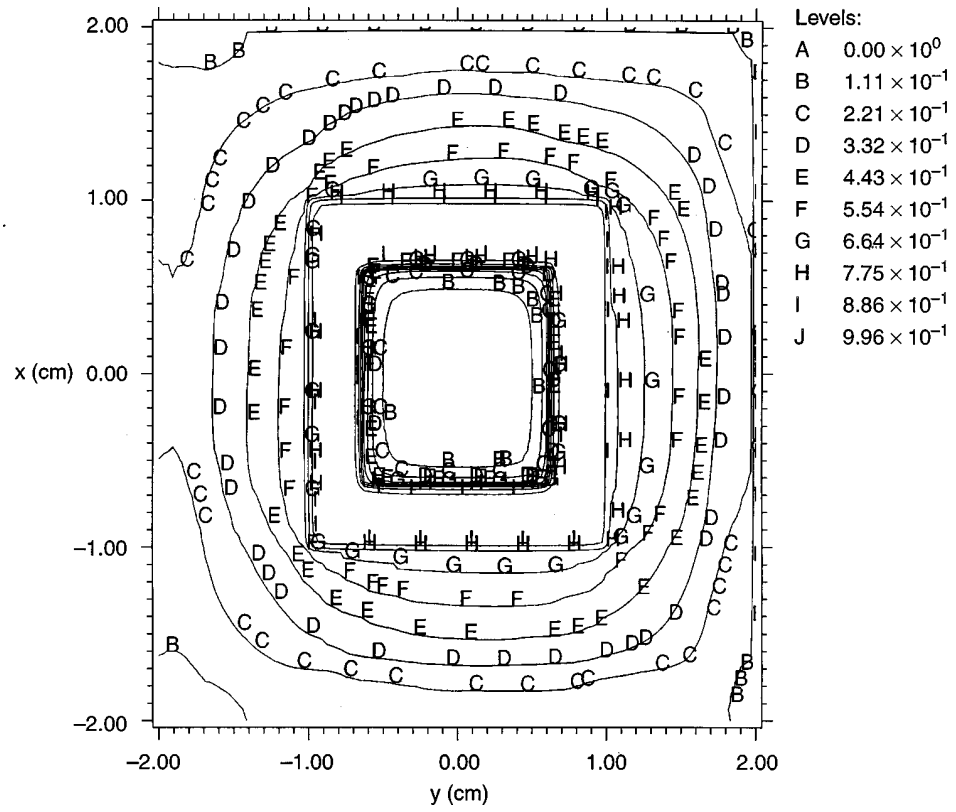

FIG. 8. Radiation distribution using the hybrid method with 40 light trajectories; there is nonzero scattering opacity.

Figure 11 shows results for the Mordant problem for $k=50\ \mathrm{cm}^{-1}$ and an average over an ensemble with ten members. Coherent structures or speckle on the scale of the wavelength $\lambda=2\pi/k$ is clearly visible. We filter the coherent ''noise'' by integrating the intensity successively over each spatial dimension using a spatial filter. For example, in the x dimension we use the Gaussian

$$F=\frac{1}{\sigma\sqrt{\pi}}\,e^{-(x-x')^2/\sigma^2}, \tag{16}$$

where we choose $\sigma=2\lambda$. The result is shown in Fig. 12. The ensemble average converges rapidly after only a few members; ten members were chosen for Fig. 12 for a comparison

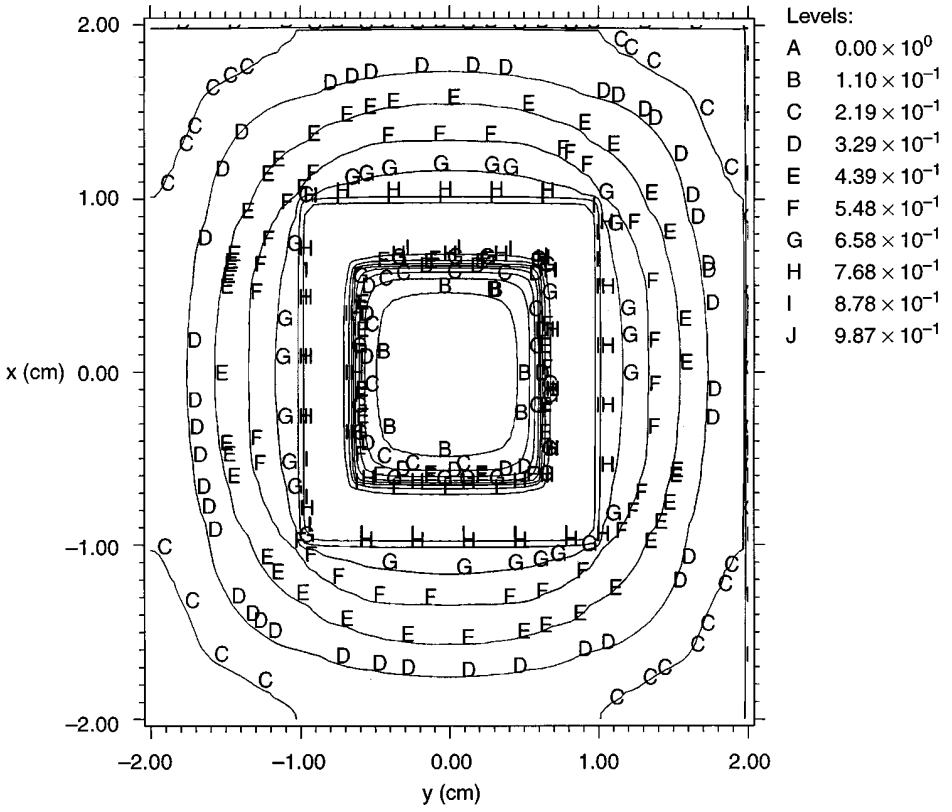

FIG. 9. Radiation distribution using the S_8 method with 8(8+2)/2 discrete quadrature points; there is nonzero scattering opacity.

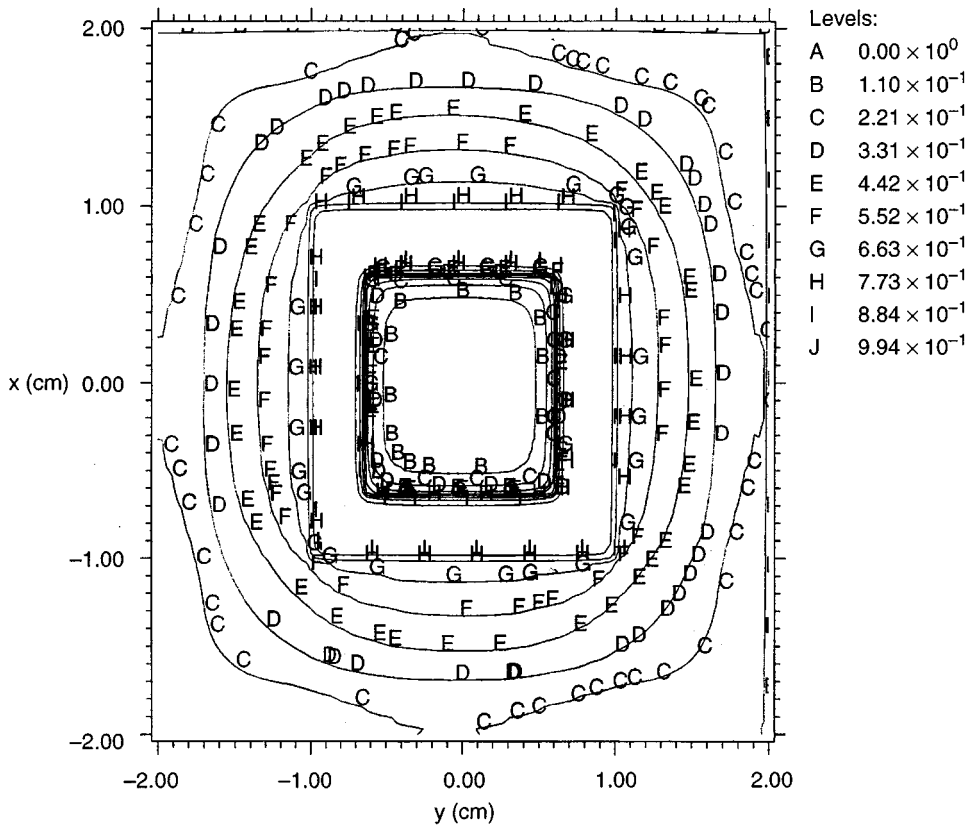

FIG. 10. Radiation distribution using the hybrid method with 500 light trajectories; there is zero scattering opacity.

with Fig. 10, which is a 500-trajectory calculation for hybrid transport, in order to point out that the transport result can be simulated with 2% or less of the storage space required by conventional transport. Note from the intensity scales, however, that there is still an irresolution close to 10% in the normalization of the source. Ray distortion is absent in the simulated transport results; however, unless an appropriate source for the wave equation [17] can be inferred from fundamental considerations, such calculations, which show a great savings in computer storage because the wave equation

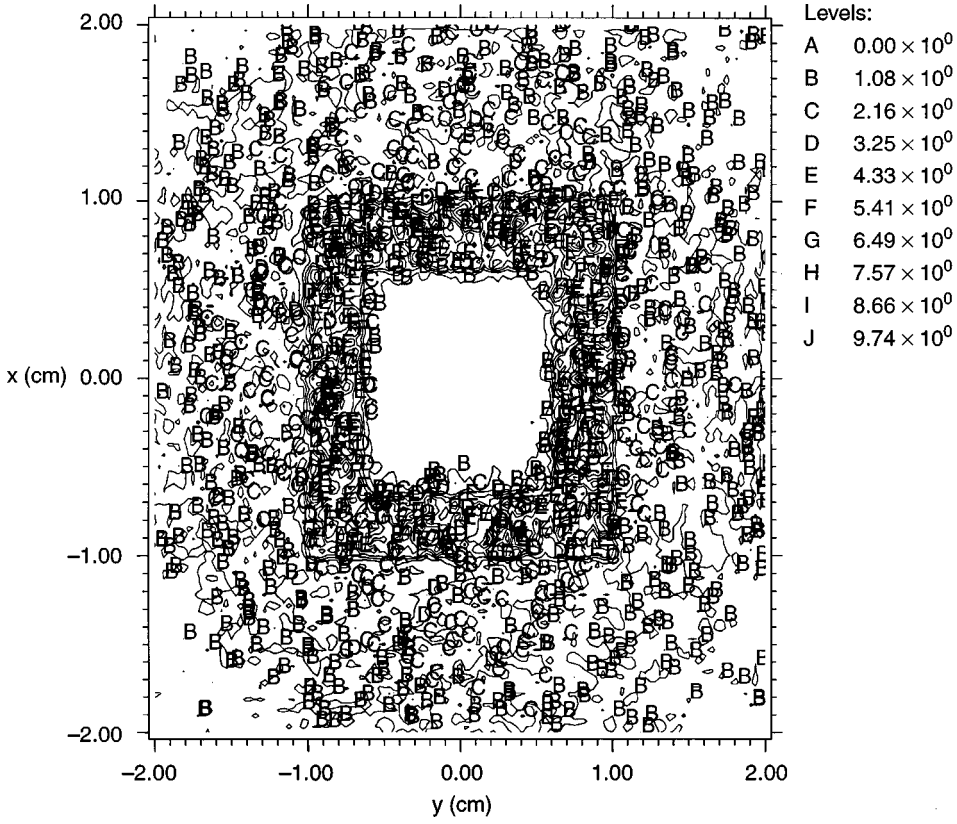

FIG. 11. Radiation distribution calculated from the wave equation with $k = 2\pi/\lambda = 50\ \text{cm}^{-1}$ (the average of a ten-member ensemble).

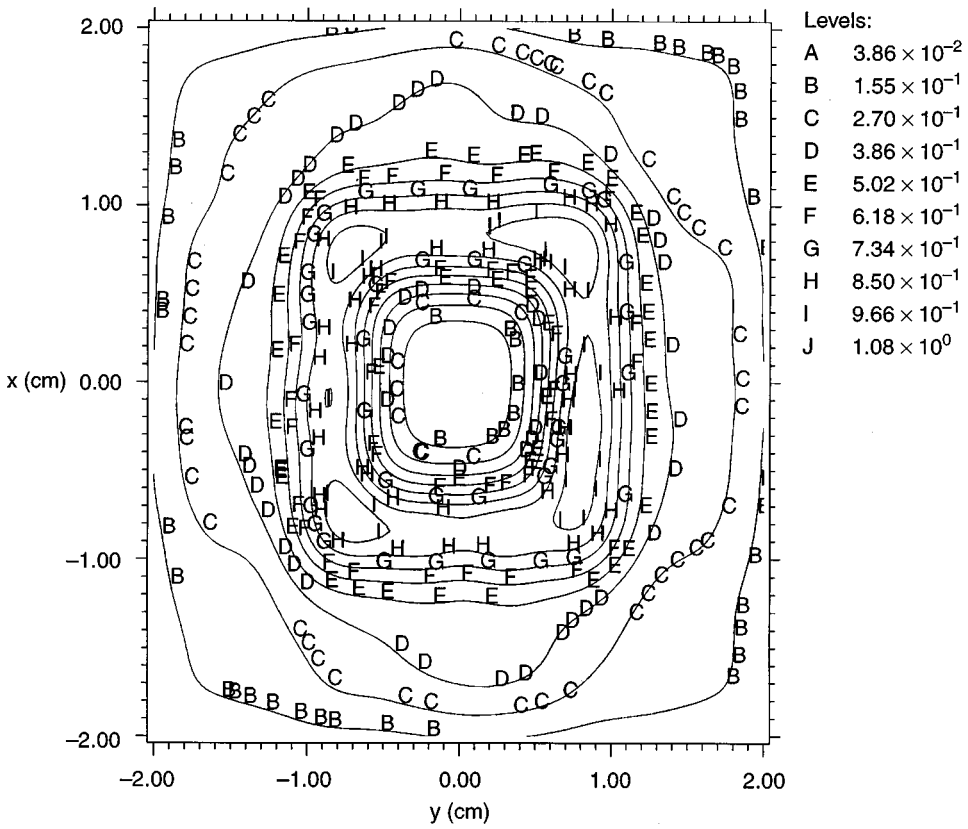

FIG. 12. Radiation distribution calculated from the wave equation with $k=2\pi/\lambda=50\ \mathrm{cm}^{-1}$ after spatial filtering (the average of a ten-member ensemble).

is undecomposed into its Fourier components, may not be of practical value. Note that we have used the wave equation to summarize the directions but not the frequencies of the light rays. The latter must still be treated as individual Fourier components represented by discrete frequency bins or groups, as in conventional transport.

Finally, we implement the algorithm given by Eqs. (5) and (6) for optically thick problems. As an example we con-

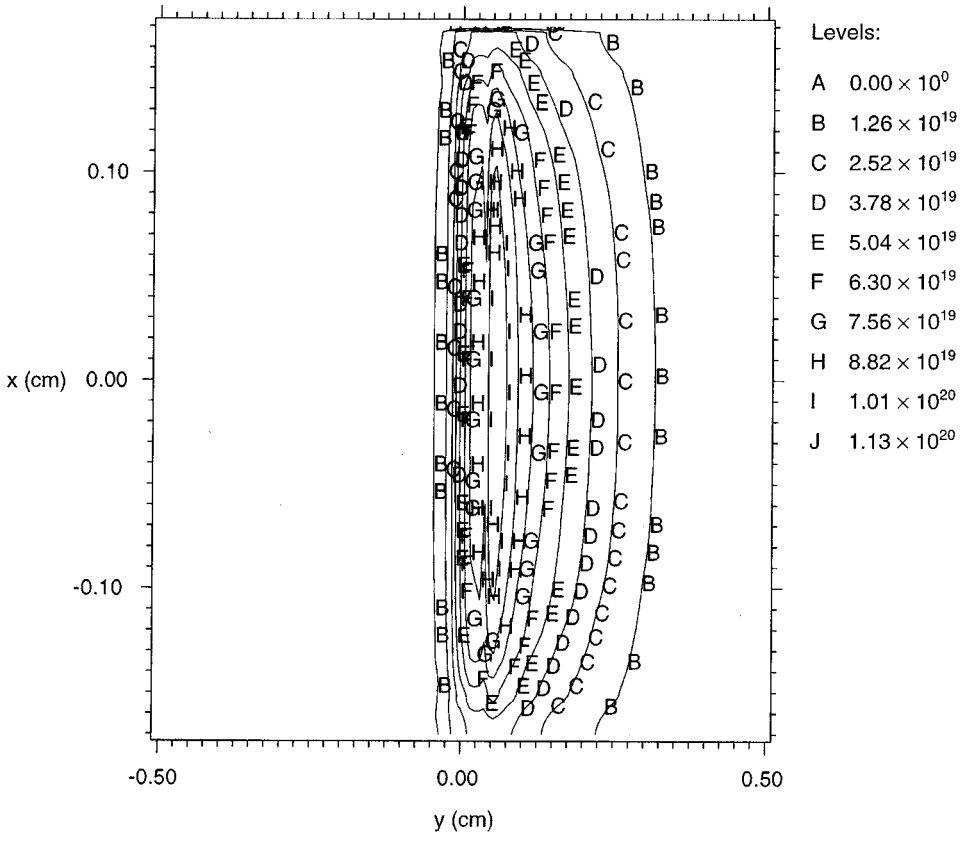

FIG. 13. Radiation flow (S_8) in a slab filled with Xe.

sider radiation flow in an x-y slab filled with Xe, as observed in an experiment [18] for which the heat capacity and density in Eq. (7) are taken to be 1.85×10^{7} ergs g^{-1} K^{-1} and 6×10^{-3} g cm^{-3}, respectively, and the Rosseland mean free path is given by the model $\lambda=9.7\times10^{-6}[T(\mathrm{eV})]^{2.2}$. The geometry of the calculation is shown in Fig. 13, in which an 80-eV Planckian source is distributed over a few zones to the right of the origin and the whole cavity is surrounded by an absorber (with three times the Rosseland mean opacity) that occupies the entire plane to the left of the origin and is 0.02 cm thick on the walls to the right of the origin. The gas to the right of the source is initially cold. The gas temperature rises according to Eq. (7) and a Planckian source distributed throughout the cavity describes gas re-emission such that radiation is transported to the right of the origin. A limit is put on the optical thickness by using an upper cutoff for the opacity at a temperature of 50 eV. As the temperature rises in the gas to a level about 10 eV lower than the radiation source temperature, the intensity of radiation has the profile shown in Fig. 13. The calculation has the same number of spatial zones as in the Mordant problem. The maximum time is given by $ct=30$ cm and 600 temporal mesh points gives acceptable accuracy. The calculation is observed to be stable down to the coarsest mesh tried, namely, 50 temporal points. In contrast, the algorithm given by Eqs. (2) and (3) is unstable for 600, but stable for 1200 temporal mesh points. This instability appears to be simply the one familiar from Euler forward differencing in ordinary differential equations, and Eq. (5b) in our split-operator scheme is effectively Euler backward or implicit differencing for this step in spanning the temporal interval. The split-operator algorithm appears to be unconditionally stable and is clearly useful for optically thick problems.

V. SUMMARY AND CONCLUSIONS

In this paper we have shown how FFT computational methods can be used to develop fast, robustly stable algorithms to solve the radiation-transport equation in both the nondiffusive and diffusive regimes. Our explicit algorithm [Eqs. (3) and (4)] is conditionally stable and thus not practical for optically thick problems; however, our split-operator implicit algorithm [Eqs. (5) and (6)] appears to be unconditionally stable.

Also a method of filling the angle space in the light-ray directions, which is a hybrid between probabilistic and deterministic theories of transport, is proposed and tested against the standard S_N method. For quite low orders ($N=4$) S_N is clearly superior to the hybrid scheme for problems with strong scattering opacity; however, for higher orders ($N=8$) the two methods appear to be very comparable in quality, with regular versus irregular ray distortion for S_N versus hybrid respectively in regions of zero scattering opacity. An advantage of the hybrid method for the higher-order calculations is the ease of choosing the light-ray directions from a random-number generator.

ACKNOWLEDGMENTS

This work was performed under the auspices of the U.S. Department of Energy by Lawrence Livermore National Laboratory under Contract No. W-7405-ENG-48. B.R. is grateful to John Castor, Britton Chang, and Merle Riley for helpful discussions.

[1] J. A. Fleck, Jr., J. R. Morris, and M. D. Feit, Appl. Phys. Lett. **10**, 129 (1976); M. D. Feit and J. A. Fleck, Jr., Appl. Opt. **17**, 3990 (1978).
[2] M. D. Feit, J. A. Fleck, Jr., and A. Steiger, J. Comput. Phys. **47**, 412 (1982).
[3] Vadim Borue and Steven A. Orszag, Phys. Rev. E **51**, R856 (1995).
[4] Pieter G. Dykema, Richard I. Klein, and John I. Castor, Astrophys. J. **457**, 892 (1996).
[5] Joel H. Ferziger, *Numerical Methods for Engineering Application* (Wiley, New York, 1981), pp. 147–152.
[6] Joel H. Ferziger, *Numerical Methods for Engineering Application* (Ref. [5]), pp. 158–167.
[7] K. Kulander, Phys. Rev. A **36**, 2726 (1987); B. Ritchie, Laser Phys. **3**, 355 (1993).
[8] B. Ritchie and M. D. Feit, Phys. Rev. E **53**, 1976 (1996).
[9] J. W. Cooley and J. W. Tukey, Math. Comput. **19**, 297 (1965).
[10] A. Burke Ritchie and Merle E. Riley, Sandia Report No. SAND97-1205, UC-401 (1997) (unpublished).
[11] E. E. Lewis and W. F. Miller, Jr., *Computational Methods of Neutron Transport* (Wiley, New York, 1984), Chap. 4.
[12] G. C. Pomraning, *The Equations of Radiation Hydrodynamics* (Pergamon, Oxford, 1973).
[13] Q. Su, J. H. Eberly, and J. Javanainen, Phys. Rev. Lett. **64**, 862 (1990).
[14] Joel H. Ferziger, *Numerical Methods for Engineering Applications* (Ref. [5]), pp. 77, 78.
[15] M. Mordant, Ann. Nucl. Energy **8**, 657 (1981).
[16] A. Icsevgi and W. E. Lamb, Phys. Rev. **185**, 517 (1969).
[17] J. C. Garrison, B. Ritchie, H. Nathel, C. K. Hong, and L. Minner, Phys. Rev. A **43**, 4941 (1991).
[18] J. C. Bozier, G. Thiell, J. P. Le Breton, S. Azra,, M. Decroisette, and D. Schirmann, Phys. Rev. Lett. **57**, 1304 (1986).